

Energy contribution of coal waste recycled with limestone to produce a Portland clinker

 D. Belkheiri^a,  S. Chhaiba^b 

a. Preparatory Classes for High Engineering Schools, (Rabat, Morocco)
b. Instituto de Ciencias de la Construcción Eduardo Torroja IETec-CSIC, (Madrid, Spain)
: salma.chhaiba@ietec.csic.es

Received 12 February 2024

Accepted 21 May 2024

Available on line 4 November 2024

ABSTRACT: Analysis has revealed that Moroccan coal gangue consists of silica, clays, and coal, making it a viable substitute for clay in clinker production. Our previous study demonstrated that the clinkering of a cement raw mix with 18.5% (wt) coal gangue and limestone produced a good Portland clinker. This clinker was close to that given by a cement raw mix of a cement plant, and which was taken as a reference-raw RR. The coal gangue contains around 8.8-11.8% coal, exhibits a calorific value of 3.77 MJ/kg and displays an exothermic effect of 67.3 J/g as determined by DSC analysis. This exothermic release is also observed in the LG cement mix. The objective of this study is to estimate the energy contribution of coal gangue in clinker production by comparing the thermochemical energy balances during clinkering up to 1450°C for the two clinker raw materials, LG and RR; our calculations indicate an energy gain of approximately 2.13%.

KEY WORDS: Coal gangue; Valorization; Clinker; Energy gain; Ecology.

Citation/Citar como: Belkheiri D, Chhaiba S. 2024. Energy contribution of coal waste recycled with limestone to produce a Portland clinker. Mater. Construcc. 74(355):e352. <https://doi.org/10.3989/mc.2024.376924>

RESUMEN: *Contribución energética de los residuos de carbón reciclados con piedra caliza para producir un clinker de Portland.* El análisis ha revelado que los residuos de carbón marroquí consisten en sílice, arcillas y carbón, lo que los convierte en un sustituto viable de la arcilla en la producción de clinker. Nuestro estudio previo demostró que la clinkerización de una mezcla cruda de cemento con un 18.5% de residuos de carbón y piedra caliza produjo un buen clinker de Portland. Este clinker fue similar al obtenido por una mezcla cruda de un cemento Portland. Los residuos de carbón contienen alrededor del 8.8-11.8% de carbón, tienen un valor calorífico de 3.77 MJ/kg y muestran un efecto exotérmico de 67.3 J/g según el análisis DSC. El objetivo de este estudio es estimar la contribución energética de los residuos de carbón en la producción de clinker mediante la comparación de los balances de energía termoquímica durante la clinkerización hasta 1450°C para los dos materiales crudos de clinker, LG y RR; nuestros cálculos indican una ganancia energética de aproximadamente 2.13%.

PALABRAS CLAVE: Residuos de carbón; Valorización; Clinker; Ganancia de energía; Ecología.

1. INTRODUCTION

In 2022, global coal consumption hit an unprecedented level of 8,415 Mt, marking a 4% rise. This increase was predominantly driven by countries like China, where coal continues to account for over 60% of electricity production. Despite efforts to diversify energy sources, coal demand in 2023 was expected to see a modest uptick of 1.4%, setting another record at approximately 8,536 Mt (1, 2). However, the downside of coal production is the substantial waste it generates, ranging from 10-15% by weight (3). This could result in more than 150 gigatons of additional waste globally, causing adverse ecological impacts on water, air, and soil. In Morocco, the closure of the Jerada coal mine in 2001 has left around 40 million tons of coal waste, leading to issues like acid mine drainage affecting groundwater. The interaction with rainwater triggers acid mine drainage (AMD), a phenomenon resulting from the oxidation of pyrite (Fe_2S) present in the coal waste. This AMD negatively affects groundwater, emphasizing the urgent need for effective environmental management and remediation strategies to mitigate the ecological consequences of coal mining activities. In general, the recycling of mining waste aligns with the principles of a circular economy, emphasizing sustainable resource utilization (4). Specifically, the recycling of coal gangue aims to exploit its mineral content, but also the coal remains it contains. China has successfully utilized coal gangue as a low-quality energy source for power generation (5). In general, the major components of coal gangue are silica, alumina, iron oxide, other oxides and carbon remains, hence a possibility of recycling in civil engineering, or energy production. Numerous scientific studies have explored its applications in cement (6), building materials (7), bricks (8) and ceramics (9).

Moreover, cement, a vital strategic material, holds a significant global production scale. In 2020, global cement consumption reached 4.17 billion tons, making concrete the second most consumed product worldwide after water, as reported by Cembureau and the United Nations (10). Understanding various stages in cement production is crucial. A study by Zhenning *et al* (11) outlines the electricity consumption distribution in a typical cement plant: extraction and crushing (5%), grinding raw materials into powder (24%), homogenization (6%), clinker burning and cooling (22%), clinker grinding (38%), and packaging and loading (5%). The cement industry is highly energy-intensive, requiring 3.2-6.3 GJ per ton of clinker (12). By 2050, energy costs for cement manufacturing are projected to represent 20-40% of total production expenses. Currently, electricity accounts for 12% of this energy consumption, but it's expected to increase

to over 20% by that year (13-14). The enormous quantities of cement produced offer the possibility of recycling industrial and construction waste. This includes the potential for recycling and recovering coal gangue, especially considering its composition containing key cement oxides.

In a previous study by Belkheiri *et al.* (15), Moroccan coal gangue was used to produce a Portland clinker. Their study involved clinkerization of a mixture of limestone-gangue at 18.5% (wt), resulting in a satisfactory Portland clinker denoted LG. The correct composition of the gangue in the limestone-gangue mixture (LG) was determined through computer simulation, aligning 11 parameters of LG with a reference raw cement plant (RR). These parameters included four oxides (CaO , SiO_2 , Al_2O_3 , Fe_2O_3), three moduli (LSF, SR, AF), and the four phases of the clinker. This current work is a continuation of the previous study, with a focus on the energy gain achieved through the combustion of the remaining coal within the cement raw limestone-gangue mixture. DSC characterization of the LG mixture revealed a combustion phenomenon occurring around 300°C-600°C. This exothermic effect has the potential to contribute to reducing energy consumption during the heat treatments of the clinker process. The ultimate goal is to achieve total recycling and recover coal waste while producing a Portland limestone-gangue clinker. The mineral components become part of the clinker, and the combustion of the organic part during the cement process could lead to a reduction in energy costs, contributing to environmental, social and economic sustainability.

2. MATERIALS AND METHODS

2.1. Used materials

The coal gangue sample was collected from various points in the backfill of Jerada's old mine in Morocco, while the limestone and raw meal originated from a cement plant. The materials and their abbreviations used are presented in Table 1.

TABLE 1. Used materials and their abbreviations.

Materials	Abbreviation
Coal gangue (coal waste) from Jerada's mine	CG
Limestone reference, used in a cement factory	LR
Cementitious mix Limestone-Gangue LGx, x=% of coal gangue by weight.	LG
Cement raw meal used in a cement plant and used as reference in this study	RR

For thermal studies, a pure coal sample is considered as a reference, denoted as PC. All materials were finely ground to a diameter of approximately 160 μm for consistency in the study.

2.2. Composition of materials

The elemental and oxide compositions of coal gangue (CG) and pure coal (PC) used in this study are derived from characterizations reported in the previous studies (15-18). The detailed compositions are presented in Table 2 and Table 3, respectively. Additionally, Table 4 provides the percentages of the studied cementitious materials, including the limestone reference (LR), cementitious mix Limestone-Gangue (LGx), and the cement raw meal reference (RR).

The mineralogical composition of the materials was determined through Rietveld quantitative X-ray diffraction (XRD) analysis. The crystalline phases identified in each material are as follows:

CG is formed by quartz 60.29%, illite ($\text{K}^+, \text{H}_3\text{O}^+$) $\text{Al}_2\text{Si}_3\text{AlO}_{10}(\text{OH})_2$:19.2%, muscovite $\text{Si}_3\text{Al}_{2.88}\text{Fe}_{0.12}\text{KO}_{12}\text{H}_2$:10.12%, clinocllore $\text{Si}_3\text{Al}_2\text{Mg}_5\text{O}_{18}\text{H}_8$: 6.8 % and gypsum 3.5%. LR is formed by calcite 80.26 %, dolomite: 12.2% and quartz 6.76%. RR is formed by calcite 63.40 %, dolomite 9.63 %, illite $\text{K}_{0.7}\text{Al}_{2.1}(\text{Si}, \text{Al})_4\text{O}_{10}(\text{OH})_2$: 13.13%, quartz 11.42% and gypsum 0.68%.

2.3. Methods

We will adopt the following methodology

- Thermal characterizations of Coal Gangue (CG) and Limestone-Gangue (LG) will qualitatively illustrate the energy contribution of CG during the heating of the cement mixture LG. The Differential Scanning Calorimetry analysis (DSC) and thermos-gravimetric analysis (TG) were performed using DSC/TG type SDTQ 600 with a heating rate of 10°C/min up to 1000°C, and using 100ml/min of dry air free of CO_2 as carrier gas.
- During the progressive heating process leading to the production of clinker, coal dispersed within the limestone-gangue mixture undergoes combustion. The combustion behavior of coal in this specific context is distinct from that in ambient air. The combustion observed during the progressive heating in the clinker production process will be assimilated to the combustion recorded in the Differential Scanning Calorimetry (DSC) analysis. The heat value derived from the combustion observed in the DSC analysis will be utilized to quantify and understand the energy contribution of coal during the clinker production.
- Based on the composition analyses, we will calculate the masses m_i of the different substances i contained in the 1kg of each clinker from the two cementitious mixtures LG and RR, these clinkers are noted LG* and RR* respectively.

TABLE 2. Elemental composition (%wt) of coal gangue CG, and pure coal PC.

Material\Elements	O	Si	Al	Fe	C	K	Mg	Na	S	Ca
CG	51.3	24.5	11.6	3.18	2.88	1.86	0.76	1.13	1.43	0.58
PC	68.6	1.8	1.13	2.94	23.1	0.168	0.013	0.115	1.55	0.29

TABLE 3. XRF composition (%wt) of coal gangue CG, and pure coal PC.

Material \Composition	C	S	A	F	M	K	N	S	P	L.O.I
CG	0.56	52.18	21.59	4.66	0.99	2.95	~0	0.97	0.08	14.22
PC	0.41	3.84	2.13	4.2	0.22	0.20	0.16	3.86	0.04	84.8

TABLE 4. Compositions (%wt) of materials and of cement raw materials.

Mat/%Compound (wt)	C	S	A	F	M	K	N	S	P	LOI	total
CG	0.56	52.18	21.59	4.66	0.99	2.95	~0	0.97	0.08	13.5	99.54
LR	50.17	4.84	1.38	0.61	1.50	0.48	...	0.14	0	40.64	99.76
RR	42.79	12.27	3.65	1.74	1.97	0.88	~0	0.34	~0	36.25	99.89

- We calculate the difference in thermochemical energy required to produce 1 kg of each of the LG* and RR* clinkers; minimizing the errors due to the approximations used.
- Energies for heating compounds:

$$E_h = \int_{T_j}^{T_k} \sum_i m_i \cdot C_{p,i}(T) \cdot dT$$
: formula (F1) where m_i is the mass of compound i and $C_{p,i}$ is the specific heat capacity at constant pressure.
- Energies related to chemical reactions denoted:
 $0 = \sum_j \nu_j A_j$ where $\nu_k < 0$ if A_k is a reactant and $\nu_k > 0$ if A_k is a product; at the temperature T_0 , and pressure $P^0=1\text{bar}$, the standard enthalpy of reaction is: $\Delta_r H^0(T_0) = \sum_k \nu_k \Delta_f H^0_{f,k}(T_0)$: formula (F₂), where $\Delta_f H^0_{f,k}$ is the standard enthalpy of formation for the compound A_k , at T_0 . At another temperature T , we calculate.

The standard enthalpy of reaction by using the following formula:

$$\Delta_r H^0(T) = \Delta_r H^0(T_0) + \int_{T_0}^T \Delta_r C_p^0(T) \cdot dT;$$

$$\Delta_r C_p^0(T) = \sum_k \nu_k C_{p,k}^0(T): (F_3).$$

The thermodynamic data, including specific heat capacities (C_p) and enthalpies of formation, will be presented in Table 6.

- Computational calculations are conducted using Python software.

3. RESULTS AND DISCUSSION

3.1. About the combustion of coal gangue and coal

Large heaps of waste coal are found at various points in the coal mine, they were generated by the industrial exploitation of the mine during 1930-2000. Figure 1 shows the largest heap, with around 20Mt of coal mining waste rocks. The distinct black color of this coal waste signifies a notable presence of coal content. Upon closer examination, stages of heating a Coal Gangue (CG) sample are illustrated in Figure 1 and it is observed that the dark color disappears at about 620 °C. This was also observed by TGA characterization, with more than 10% of loss of mass due to the combustion of coal residues. The thermal characterizations of CG show an exothermic contribution attributed to the combustion of the coal. According to a mine staff report, the calorific value of gangue (CVCG) is determined to be 3.767 MJ/kg. This value aligns with the literature, where reported values fall within the range of 2.307 to 8.309 MJ/kg (18); and the calorific value of this anthracite coal is approximately 31.8 MJ.kg⁻¹. From these values, we can deduce an estimation of 11.8% coal in the coal gangue. Based on the ratio of carbon atoms in the gangue and in the coal reported in Table1, we can estimate a percentage of 12.4% coal in the CG. This estimation aligns with findings from a study by Taha *et al* (18, 19), where the content of coal in coal gangue is reported to be within the range of 10-15%. Moreover, the study suggests that coal extraction through flotation yields a percentage higher than 6.09%, with an extraction efficiency of 60%.

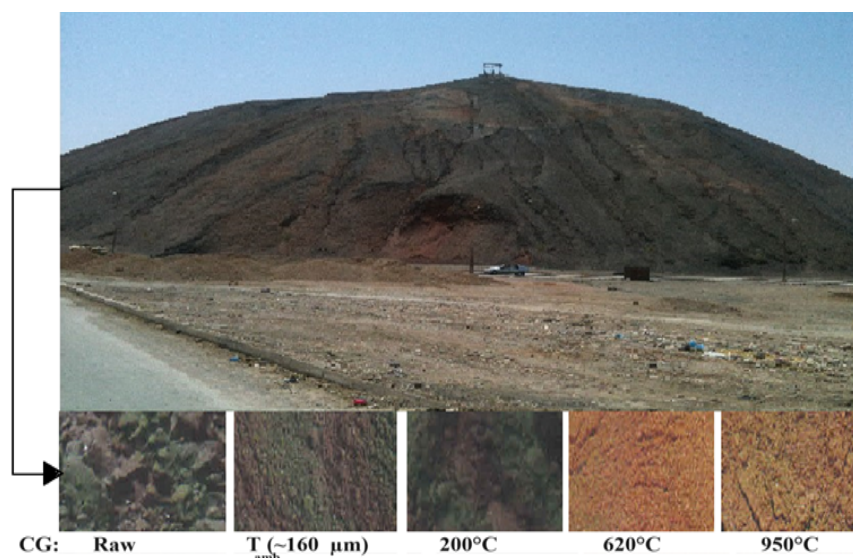


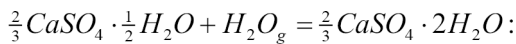
FIGURE 1. The studied sample of CG is extracted from backfill of coal gangue in Jerada's mine; Some stages of its heating from ambient temperature to 950°C.

3.2. Thermal characterizations

3.2.1. DSC characterization of coal gangue CG compared to the pure coal PC

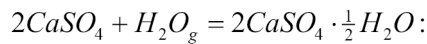
The DSC analyses of coal gangue CG compared to the pure coal PC are presented by in Figure 2; the heating rate was 10 °C/min under air.

The DSC analysis of coal gangue shows an endothermic region occurring between 100°C-150°C attributed to the evaporation of free water. Additionally, two dehydration processes, specifically from gypsum to plaster and then to anhydrite:



$$\Delta_r G_1^0(T, kJ / mol) = -55.53 + 0.1460T$$

and



$$\Delta_r G_2^0(T, kJ / mol) = -62.20 + 0.1491T$$

They are theoretically expected to occur at 106°C and 153°C, respectively: Comparing these theoretical values to those reported in literature (20), the temperature for the first dehydration aligns closely, with literature reporting 105°C. However, for the second dehydration, the literature reports a slightly higher temperature of 175°C.

At 580°C, the coal gangue (CG) undergoes a polymorphic transformation of quartz: $SiO_{2\alpha} \rightarrow SiO_{2\beta}$.

At 580°C, we have the polymorphic transformation of quartz: $SiO_{2\alpha} \rightarrow SiO_{2\beta}$. Then, in the range 300–600°C, an exothermal effect is observed, mainly attributed to the combustion of coal.

Using the DSC characterization (10°C/min, in air) for CG, we obtain the combustion enthalpy of CG is $H_{CG} = -63.74 \text{ J.g}^{-1}$; this value is used in the thermochemical balance calculations for the cementitious mixture LG. It's important to note that this value represents a minimum estimate, as the observed exothermic effect persists across multiple heating and cooling cycles, indicating incomplete combustion. This persistence is demonstrated in Figure 2(b), where the PC sample exhibits the observable exothermic effect even after five cycles of heating and cooling.

3.2.2. Thermal characterizations of materials CG and LG.

Characterizations of materials LG and CG was done using thermogravimetric TGA and thermo-differential TDA analyses. The graphical representations of these analyses are illustrated in Figure 3.

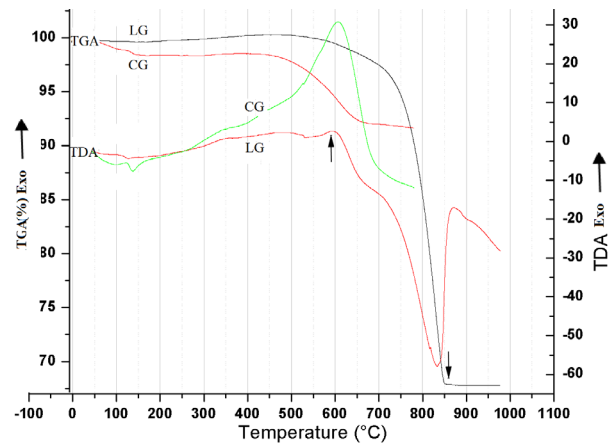


FIGURE 3. TGA and TDA for coal gangue CG and for the cementitious mixture LG.

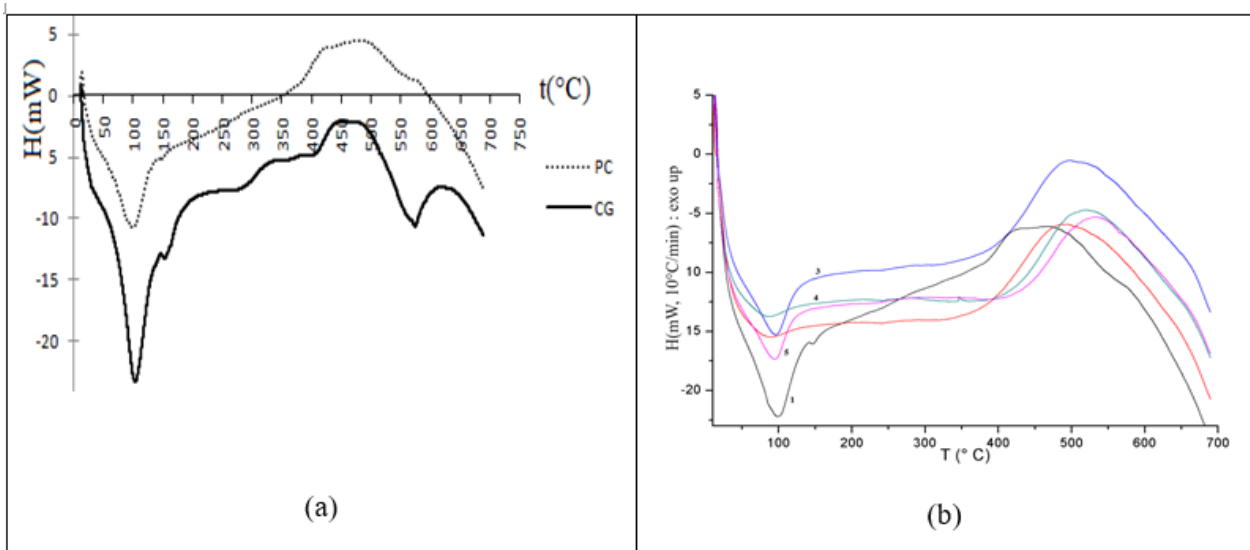
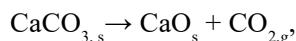


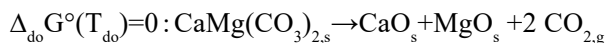
FIGURE 2. Comparatives curves of DSC; (a) for CG and PC, (b) DSC curves after successive heating of a pure coal (11.3mg).

In the temperature interval of 300-600°C, we observe the presence of the exothermic effect due, mainly, to the combustion of coal in the coal gangue, this effect is also noticeable in the limestone-gangue cementitious mixture LG. At about 850°C (P=1 bar), we observe a main endothermic peak attributed to the calcination of the limestone, in the LG mixture:



At this temperature the standard free enthalpy of this equilibrium verifies the condition $\Delta_{\text{ca}} G^\circ(T_{\text{ca}}) = 0$: $\Delta_{\text{ca}} G^\circ(T) = 178.2 - 0.1601 \cdot T$ (kJ.mol⁻¹), $T_{\text{ca}} = 1113\text{K}$ (840°C).

Similarly, the temperature at which dolomite decomposes is determined, considering a hypothetical single-stage decomposition:



The standard free enthalpy of this equilibrium is:

$$\Delta_{\text{do}} G^\circ(T) = 279.1 - 0.3356 \cdot T \text{ (kJ.mol}^{-1}\text{)}$$

This reaction occurs at $T_{\text{do}} \approx 831\text{K}$ (558°C). Adopting a two-step decomposition, as reported in some literatures (21); the process involves the initial formation of MgO, CO₂, and calcite at the temperature of 750°C, followed by the subsequent decarbonation of calcite around 900°C.

A DSC characterization has been done under argon atmosphere for the mixtures LG and RR; therefore, the thermal effects excluding combustions can be seen; thus, we will consider that the combustion phenomenon, in the LG mixture, is predominant in front of other reactions taking place in the interval 300-600°C. The comparative results are reported in Figure 4.

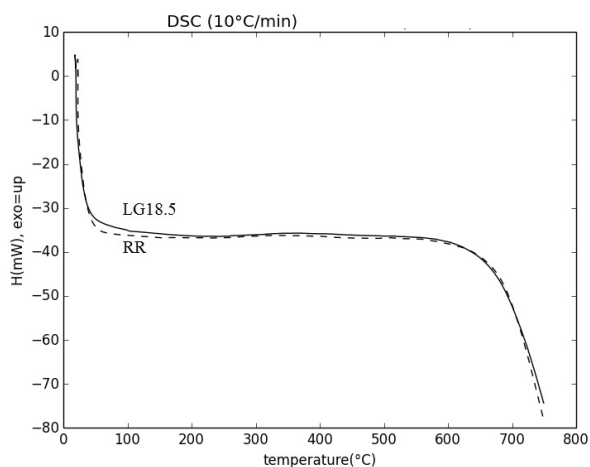


FIGURE 4. DSC analysis for the cement raw LG and RR mixtures.

The thermal behavior of the two mixtures, LG and RR, exhibits notable similarities. Two endothermic phenomena are observed:

- Water Losses: Involving both free water and the dehydration of gypsum.
- Calcination of Calcite: The endothermic process where calcium carbonate (calcite) is converted into calcium oxide and carbon dioxide

It's important to note that limestone typically contains dolomite (calcium magnesium carbonate), which undergoes calcination around 500°C. Additionally, around 550°C, the decomposition of clays initiates through dehydrations, dehydroxylations, and decompositions (22). These reactions continue until approximately 900°C.

The main thermochemical events involve the heating of all substances, and the main reactions are: decomposition of calcite and dolomite, combustion of coal residues, decomposition of clays and formation of the four phases of clinker. In addition to these primary events, there are, also, minor thermal occurrences like the alpha-beta transition of silica and dehydration of gypsum, and polymorphism in phases of clinker. In the literature, these main physicochemical phenomena take place in temperature intervals (23). Due to the complexity of these physicochemical phenomena, detailed studies are challenging, and approximations become necessary. To facilitate analysis, relevant temperatures $T_{r=1,2,\dots}$ are introduced, corresponding to the key reactions. For instance, the combustion phenomena of coal begins at 727K as showed in thermal characterization and in literature (24); the $\alpha\beta$ transformation of quartz occurs at 848K. $T_0 = 298\text{K}$ is the initial temperature and $T_7 = 1723\text{K}$ is the final temperature of clinkerization.

We study mass and energy balances during the production of LG* and RR* clinkers, from raw materials. These balances are examined for different stages as presented in the Table 5:

Stage I: the first stage of decomposition.

Stage II: the second stage of clinkerization.

Overall balance:

In the energy balance analysis, the focus is on the algebraic determination of energies required to produce 1 kg of clinkers denoted LG* and RR*. We are interested in the difference of the energies $\Delta E = E_{LG} - E_{RR}$, in this way we will reduce the impact of approximations done. Moreover, since the limestone LR is the same for both raw feeds, certain terms in the balance are inherently similar.

We present the balance involving the main thermochemical transformations. These include

TABLE 5. Main considered reactions, transformations and temperatures.

	Temperature (K)	Number j of : reaction or transformation	Enthalpy : $\Delta_j H^\circ$ or L_i at T_i (kJ/mol)
Decomposition : stage I	$T_1=379$	1 : $C\underline{S}H_2 \rightarrow C\underline{S}H_{0.5}+1.5H$	+150
	$T_2=426$	2 : $C\underline{S}H_{0.5} \rightarrow C\underline{S}+0.5H$	-95.10
	$T_3=727$	3 : $\frac{‘C_x H_y O_z S_1’+a O_2 + 4a N_2}{\text{minor reactions in CG}} \rightarrow C+H+SO_2 +4aN_2$	-63.74 (J/g CG)
	$T_4=848$	4 : $S_\alpha \rightarrow S_\beta$	+0.518
	$T_5=1023$	5 : $CMC_2 \rightarrow M+C+CC$	+120.7
	$T_6=1173$	6 : $CC \rightarrow C+C$	+165.5
	$T_6=1173$	7 : Illite $S_3A_{1.55}K_{0.35}H \rightarrow$ oxides	+249.9
	$T_6=1173$	8 : Muscovite : $S_3A_{1.5}F_{0.06}K_{0.5}H \rightarrow$ oxides	+337.4
	$T_6=1173$	9 : Clinocllore $S_3A_1M_5H_4 \rightarrow$ oxides	+475.6
Clinkerization : stage II	$T_6=1173$	10 : $2C+S_\beta \rightarrow C_2S_\gamma$	-136.9
	$T_6=1173$	11 : $C_2S_\gamma \rightarrow C_2S_{\alpha'}$	+13.70
	$T_7=1373$	12 : $3C+A \rightarrow C_3A$	+4.500
	$T_7=1373$	13 : $4C+A+F \rightarrow C_4AF$	-108.3
	$T_8=1573$	14 : $C+C_2S_{\alpha'} \rightarrow C_3S$	+15.52
	$T_9=1723$	End of clinkerization	

the heating energies for the main compounds in the temperature intervals considered (Formula F1), as well as the enthalpies of the chemical reactions listed in Table 5 (Formulas F2 and F3). The heats of change of physical state or of polymorphism are included with those of the reactions presented in Table 5.

$$\Delta E = E_{LG^*} - E_{RR^*} = \left(\sum_{i=1}^9 \Delta E r_{i,I} + \Delta E h_{s,I} + \Delta E h_{g,I} \right) + \left(\sum_{i=10}^{14} \Delta E r_{i,II} + \Delta E h_{s,II} + \Delta E h_{l,II} + \Delta E h_{g,II} \right)$$

Where $\Delta E r_{i,I}$ or II' , $\Delta E h_{s,I}$ or II' , $\Delta E h_{l,I}$ or II' and $\Delta E h_{g,I}$ or II' are respectively the differences in energies of: reactions and heating of solids s, liquids l and gases g in stages I and II.

The terms of heating are of the form: $\int_{T_j}^{T_k} \sum_i \Delta m_i \cdot C_{pi}(T) \cdot dT$ in general, for a given substance i, the massic heat capacity is:

$$C_{p,i}(T) = a_{-2,i} T^{-2} + a_{-1} T^{-1} + a_{-0.5,i} T^{-0.5} + \sum_{k=0}^4 a_{k,i} T^k$$

The data on the specific heat capacity $C_{p,i}$ shown in Table 5 is given in literature, mainly from the NASA/TP-2002-211556 report (25) and other sources (26-36). The specific heat capacity of coal is reported based on the work of Lesniak *et al* and Eisermann *et al* (28, 29), it is formed by two contributions of fixed carbon FC (fraction m_C , C_{pC}) and volatile matter (fraction $1 - m_C$, C_{pV}). In our case, for anthracite, the value is $FC=93$ and $VM=5$ (37).

Using formula (F_1), we calculate the heating of all solids, liquids and gases; the gases CO_2 , H_2O , SO_2 , O_2 , and N_2 are involved in the reactions of calcinations of calcite and dolomite, dehydrations of gypsum, decomposition of clays and combustion of coal.

3.3. Mass and energy balances for the production of 1 kg LG^* and RR^* clinkers

XRF and XRD data are cross-referenced to give the mass fractions of the compounds in the three materials CG, LR and RR. Amorphous compounds, not visible, are considered, and total oxide content from XRD is adjusted to match XRF values.

TABLE 6. Specific massic heat values ($\text{J}\cdot\text{K}^{-1}\text{ Kg}^{-1}$), masses (kg), molar masses ($\text{kg}\cdot\text{mol}^{-1}$) and standard, enthalpies of formation ΔH° ($T_0=298\text{K}$, $\text{kJ}\cdot\text{mol}^{-1}$).

Comp	a_{-2}	a_{-1}	$a_{-0.5}$	a_0	a_1	a_2	a_3	a_4	Δm	M	Hmol	References
calcite (T<500)	-1,11E+09	2,08E+07	0,00E+00	-1,59E+05	6,33E+02	-1,38E+00	1,56E-03	-7,25E-07	2,74E-02	1,00E-01	-1,21E+03	(25)
calcite	-2,15E+07	0,00E+00	0,00E+00	9,95E+02	2,71E-01	0,00E+00	0,00E+00	0,00E+00	2,74E-02	1,00E-01	-1,21E+03	(26)
illite	-1,81E+07	0,00E+00	0,00E+00	8,63E+02	5,97E-01	0,00E+00	0,00E+00	0,00E+00	-1,64E-01	3,89E-01	-5,97E+03	(26)
muscovite	-1,76E+07	0,00E+00	0,00E+00	8,42E+02	5,82E-01	0,00E+00	0,00E+00	0,00E+00	2,22E-02	4,02E-01	-5,97E+03	(26)
clinochlore	-3,20E+07	0,00E+00	0,00E+00	1,14E+03	5,09E-01	0,00E+00	0,00E+00	0,00E+00	1,49E-02	5,56E-01	-8,91E+03	(25)
quartz-a	-8,00E+07	1,00E+06	0,00E+00	-4,36E+03	1,03E+01	-1,20E-03	-1,50E-05	1,15E-08	3,94E-02	6,01E-02	-9,11E+02	(25)
quartz-b	3,21E+06	0,00E+00	0,00E+00	9,74E+02	1,72E-01	0,00E+00	0,00E+00	0,00E+00	3,94E-02	6,01E-02	-9,11E+02	(27)
dolomite	1,50E+05	0,00E+00	-3,55E+04	2,97E+03	-9,09E-01	4,18E-04	0,00E+00	0,00E+00	4,04E-03	1,84E-01	-2,33E+03	(28,29)
coal	0,00E+00	0,00E+00	0,00E+00	-8,91E+01	3,67E+00	-1,63E-03	0,00E+00	0,00E+00	3,16E-02	1,80E-02	0,00E+00	(30, 31, 32)
gypsum	0,00E+00	0,00E+00	0,00E+00	5,29E+02	1,85E+00	0,00E+00	0,00E+00	0,00E+00	1,06E-03	1,72E-01	-2,02E+03	(30, 31, 32)
plaster	0,00E+00	0,00E+00	0,00E+00	3,25E+03	1,13E+01	0,00E+00	0,00E+00	0,00E+00	9,42E-04	1,43E-01	-1,58E+03	(25)
anhydrite	-1,82E+07	0,00E+00	0,00E+00	8,30E+02	3,58E-01	0,00E+00	0,00E+00	0,00E+00	8,37E-04	1,36E-01	-1,43E+03	(25)
T	-1,78E+05	2,83E+04	0,00E+00	6,21E+01	2,00E+00	-2,77E-03	1,89E-06	-5,08E-10	0,00E+00	7,99E-02	-3,05E+02	(25)
P	-1,76E+06	-2,69E+03	0,00E+00	4,09E+02	1,69E+00	-1,82E-03	9,63E-07	-2,03E-10	0,00E+00	1,42E-01	-1,12E+03	(25)
C	-2,17E+07	0,00E+00	0,00E+00	1,07E+03	-2,91E-01	1,92E-04	-3,08E-08	0,00E+00	2,51E-03	5,60E-02	-6,35E+02	(25)
A	-4,92E+07	0,00E+00	0,00E+00	1,20E+03	6,74E-02	0,00E+00	0,00E+00	0,00E+00	1,79E-02	1,02E-01	-1,68E+03	(25)
F	-9,33E+06	0,00E+00	0,00E+00	6,14E+02	4,88E-01	0,00E+00	0,00E+00	0,00E+00	-7,42E-03	1,60E-01	-8,24E+02	(25)
F>600K	-9,33E+06	0,00E+00	0,00E+00	6,14E+02	4,88E-01	0,00E+00	0,00E+00	0,00E+00	-7,42E-03	1,60E-01	-8,24E+02	(25)
M	-2,43E+07	0,00E+00	0,00E+00	1,15E+03	2,26E-01	-1,01E-04	2,60E-08	0,00E+00	-8,78E-03	4,03E-02	-6,02E+02	(25)
K	0,00E+00	0,00E+00	0,00E+00	1,06E+03	0,00E+00	0,00E+00	0,00E+00	0,00E+00	3,23E-04	9,42E-02	-3,62E+02	(25)
N	3,42E+07	-3,40E+05	0,00E+00	2,23E+03	-1,65E+00	2,07E-03	-1,08E-06	2,34E-10	0,00E+00	6,20E-02	-4,15E+02	(25)
CO ₂	2,22E+07	-3,38E+05	0,00E+00	1,57E+03	-1,74E-02	9,19E-07	-3,57E-10	1,20E-13	7,92E-02	4,40E-02	-3,94E+02	(25)
H ₂ O	4,78E+08	-1,11E+06	0,00E+00	2,15E+03	1,06E+00	-3,16E-04	4,35E-08	-2,23E-12	1,21E-02	1,80E-02	-2,42E+02	(25)
SO ₂	-6,89E+06	1,18E+05	0,00E+00	-3,06E+02	2,86E+00	-3,26E-03	1,88E-06	-4,37E-10	1,68E-03	6,40E-02	-2,97E+02	(33)
C ₃ S	-2,86E+05	0,00E+00	-1,21E+04	1,46E+03	-1,02E-02	0,00E+00	0,00E+00	0,00E+00	-9,26E-04	2,28E-01	-2,93E+03	(33)
C ₂ Sg	-1,37E+07	0,00E+00	9,63E+03	0,00E+00	1,24E+00	-4,74E-04	0,00E+00	0,00E+00	-1,19E-03	1,72E-01	-2,32E+03	(33)
C ₂ Sap	0,00E+00	0,00E+00	0,00E+00	9,40E+02	0,00E+00	1,10E-04	0,00E+00	0,00E+00	-1,19E-03	1,72E-01	-2,31E+03	(33, 34)
C ₃ A	1,86E+07	0,00E+00	0,00E+00	9,65E+02	1,77E-02	0,00E+00	0,00E+00	0,00E+00	3,74E-03	2,70E-01	-3,59E+03	(33, 35)
C ₄ AF	1,12E+07	0,00E+00	0,00E+00	7,70E+02	3,74E-02	0,00E+00	0,00E+00	0,00E+00	-1,11E-03	4,86E-01	-5,08E+03	(25)
FeO	-1,38E+07	-4,20E+04	0,00E+00	6,39E+02	-1,15E-01	5,07E-05	-7,86E-09	4,21E-13	0,00E+00	7,18E-02	-2,72E+02	(25)
O ₂	-8,90E+06	1,26E+05	0,00E+00	2,91E+02	1,12E+00	-1,78E-04	-5,26E-07	2,70E-10	5,53E-02	3,20E-02	0,00E+00	(25)
N ₂	6,56E+06	-1,13E+05	0,00E+00	1,81E+03	-2,53E+00	4,11E-03	-2,86E-06	7,48E-10	1,94E-01	2,80E-02	0,00E+00	(25)
H ₂ OI	-2690906	0	485,00939	1,1057984	-0,000848	0	0	0	0,00247	0,018	-241,826	(19)

3.3.1. Massic compositions of coal gangue CG, limestone LR, and cement mixtures LG and RR

The coal gangue consists of various compounds, including quartz, illite, muscovite, clinochlore, gypsum, ferric oxide (F), and sulfur dioxide (SO₂). These compounds are derived, in part, from pyrite, which makes up approximately 2-5% of the coal (38). In the analysis of coal gangue (CG), adjustments are made to align the total amount of oxides 'CSAMKS' given by XRD (94.51%), to that given by XRF

(79.24%). The experimental percentage of coal in the gangue is estimated using the loss on ignition L.O.I, which is formed by dehydration of the three water-bound in clays and gypsum (2.39 %). This estimation suggests a maximum coal content approaching 11.85%, consistent with previous estimates. For different samples of gangue, the losses on ignition varied between 10.6 and 14.22, corresponding to a coal content between 8.8 and 11.8%. For the mass balance, the study uses the conservative assumption of 11.85 % coal in GC.

The gases released during combustion include water vapor, carbon dioxide, and sulfur dioxide. In this study, we use the experimental amounts of CO₂ and SO₂ estimated by Taha *et al*: 0.243 kg CO₂ and 0.00628 kg SO₂ per kg of gangue and we obtain the amount of water vapor released from an approximate ‘formula’ of the anthracite. Coal can be modeled by the formula ‘C_xH_yO_zS_tN_u’. Jerada’s anthracite analysis indicates volatile matter (VM) at about 5%, fixed carbon (FC) at approximately 93%, and ash (ASH) at 5.5.

A model proposed by Shen *et al* (39) and reported in Lawal *et al*’s study (40) provides an approximate formula (‘C₁H_{1.158}O_{0.418}N_uS_t’). This model predicts that the combustion of 1 ton of CG produces 62.1 kg H₂O and 263 kg CO₂. The optimal limestone-gangue mixture retained has a composition of 17.1% coal gangue. The massic composition of coal gangue is given in Table 7.

We complete the determination of the mass fractions of the main compounds forming the LR and RR materials. The total amount of carbon dioxide from calcite and dolomite, and from the XRD analysis we obtain the ratios of calcite to dolomite and to quartz: 6.58 and 11.9 respectively. For the LR material, the total 96.089% in CMC given by XRD is adjusted to 74.865% given by XRF; and for the RR material the total of L.O.I is composed of carbon dioxide and water of clay, maintaining the same ratio, 6.58, of CC to CMC. All the results are reported in Table 7 and used to determine the energies involved in the comparative energy balance of the two cement mixtures LG, and RR.

3.3.2. Energy balance

The masses of the gases I: CO₂, H₂O, SO₂, O₂ and N₂ concerned by this phase I are respectively: 66.14, 16.81, 1.682, 55.04, 192.7 gram for 1 kg of clinker. For the energy balance, the solids in this phase are denoted solids I.

During the clinkering phase, the oxide compositions (XRF) of the two mixtures are used to calculate the saturation factor lime moduli LSF=100C/(2.8S+1.65A+0.35F), the ratio SR=S/(A+F) as well as the four phases of the clinker and possibly, the percentage of free lime Cf. In order to calculate compositions of the four phases, we use the Taylor’s matrix (41) leading to the system of equations:

After calculating the total mass of the four phases (solids II), we assumed that the difference with the mass of the C-S-A-F oxides was that of the free lime, in order to adjust the total mass. The theoretical percentage of free lime can be approximated using Fundal’s empirical equation: % CaO_(free)=0.31 (LSF-100)+2.18 (SR-1.8)+(0.73 Q₄₅ + 0.33 C₁₂₅ + 0.34 Aq). The total amount of C₂S formed at 1173K will be distributed between the final masses of C₂S and that of C₃S which will form at 1573 K; these two masses are obtained by the Taylor model above.

In Table 8, we give the massic composition of these four phases, anhydrite, minor oxides and the gases. All the results are used to determine the energies involved in the comparative energy balance of the two cement mixtures LG and RR.

TABLE 7. Energy balance of the first phase I (calcinations-decomposition).

	CC	il	mu	cn	qu	CMC2	CSH2 (T<T1)	coal	A	F	M	K	N	T	P	s	LOI	tot
CG	0,00	15,73	8,29	5,57	49,40	0,00	2,87	11,8	0,00	4,47	0	0	0	0	0,08	0	14,22	98,20
LO	78,66	0,00	0,00	0,00	6,62	11,95	0,30	0,00	1,38	0,61	0	0	0	0	0,00	0	40,64	99,52
LG17,1	65,21	2,69	1,42	0,95	13,94	9,91	0,74	2,02	1,14	1,27	0	0	0	0	0,01	0	36,12	99,30
RR	63,33	13,12	0,00	0,00	11,40	9,63	0,67	0,00	0,00	1,74	0	0	0	0	0,00	0	36,25	99,89
1kgLG*	1,02	0,04	0,02	0,01	0,22	0,16	0,01	0,03	0,02	0,02	0	0	0	0	0,00	0	0,57	0,99
1kgRR*	0,99	0,21	0,00	0,00	0,18	0,15	0,01	0,00	0,00	0,03	0	0	0	0	0,00	0	0,57	1,00
Δm	2,74E-02	-1,64E-01	2,22E-02	1,49E-02	3,94E-02	4,04E-03	1,06E-03	3,16E-02	1,79E-02	-7,42E-03	0	0	0	0	2,14E-04	-3,14E-03	-6,10E-03	

TABLE 8. Energy balance of the second phase II of clinkerization.

	C ₃ S	C ₂ S	C ₃ A	C ₄ AF	M	K	N	T	P	CS	LOI	C free	tot	CO ₂	H ₂ O	SO ₂
LG*	6,45E+01	2,32E+01	3,84E+00	1,41E+00	2,21E+00	1,41E+00	0	0	2,14E-02	7,50E-01	5,65E+01	1,28E+00	9,79E+01			
RR*	6,46E+01	2,33E+01	3,47E+00	1,52E+00	3,09E+00	1,38E+00	0	0	0,00E+00	9,07E-01	5,69E+01	1,58E+00	9,83E+01			
Δm(1kg*)	-9,26E-04	-1,19E-03	3,74E-03	-1,11E-03	-8,78E-03	3,23E-04	0	0	2,14E-04	-1,56E-03	-3,14E-03	-2,98E-03	-3,83E-03	7,92E-02	1,22E-02	1,68E-03

Finally, in Table 9, we present the energy balance of the reactions and the heating, then we deduce the overall balance; these results are generated by the program Python.

TABLE 9. Summary of energy balances and estimate of relative gain or efficiency.

	Transformation	E(LG*)-E(RR*)
	dEr1(gypsum)=	924
	dEr2(plaster)=	-626
	dEr3(coal)=	-17063
	dEr4(quartz-ab)=	410
	dEr5(dolomite)=	2647
	dEr6(calcite)=	49045
Phase I	dEr7(illite)=	-105092
	dEr8(muscovite)=	18642
	dEr9(clinocllore)=	12765
	dErI=	-38349
	dEhs1=	-85435
	dEhg1=	135517
	dEhI=	50082
	dEI=	11733
	dEr10(C2Sgamma)=	1500
	dEr11(C2Sgammalphaprime)=	-150
	dEr12(C3A)=	62
	dEr13(C4AF)=	248
	dEr14(C3S)=	-63
Phase II	dErII=	1597
	dEhs21=	-380
	dEhs22=	-180223
	dEhg2=	82073
	dEhII=	-98530
	dEII=	-96933
	dEtot	-85200
	Yield(%)	2,13

4. CONCLUSIONS

This study highlights the energy contribution of coal combustion as a prime material for clinker production. Regarding energy considerations, the following conclusions can be drawn:

1. The combustion of the coal contained in the gangue is more difficult than that in the open air,

because this combustion takes place within the LG cement mixture; for this reason, the value of the enthalpy of combustion, during the DSC, can be used to estimate the energy input, but the heating rate is very high in the cement industry where the calcination temperature rises to 900°C in a few minutes. The efficiency of this energy input is improved by favorable kinetics resulting from the small particle size and consequently larger surface area.

2. Coal combustion generates heat within the limestone-gangue mixture itself during the first phase of clinker's elaboration effectively improving calcination; this internal heat is added to that received by conduction and convection. On the other hand, using the approximation of an adiabatic transformation, it is possible to present the energy gain as a lowering of the working temperature.
3. Incorporating coal waste in cement production offers economic and ecological benefits, potentially making the industry more sustainable. As this practice gains traction, it's crucial to address associated social challenges. Effective collaboration among industry stakeholders, policymakers, and communities is key for ensuring both sustainability and social responsibility in cement production.

Authorship contribution statement

Driss Belkheiri: Conceptualization, Data cleansing, Formal analysis, Research, Project administration, Software, Write - original draft, Resources.

Salma Chhaiba: Research, Methodology, Supervision, Write - review & editing.

Declaration of competing interest

The authors of this article declare that they have no financial, professional or personal conflicts of in-terest that could have inappropriately influenced this work.

REFERENCES

1. Coal 2023. Analysis and forecast to 2026. Retrieved from https://iea.blob.core.windows.net/assets/a72a7ffa-c5f2-4ed8-a2bf-eb035931d95c/Coal_2023.pdf
2. Bp Energy Outlook. 2023 edition. Retrieved from <https://www.bp.com/content/dam/bp/business-sites/en/global/corporate/pdfs/energy-economics/energy-outlook/bp-energy-outlook-2023.pdf>
3. Li J, Wang J. 2019. Comprehensive utilization and environmental risks of coal gangue: A review. J.

- Clean. Prod. 239:117946. <https://doi.org/10.1016/j.jclepro.2019.117946>
4. Tayebi-Khorami M, Edraki M, Corder G, Golev A. 2019. Re-thinking mining waste through an integrative approach led by circular economy aspirations. *J. Minerals*, 9(5):286. <https://doi.org/10.3390/min9050286>.
 5. Yu JL, Meng FR, Li XC, Tahmasebi A. 2012. Power generation from coal gangue in China: Current status and development. *J. Open J. Adv. Mater.* 550:443-446. <https://doi.org/10.4028/www.scientific.net/AMR.550-553.443>
 6. Shuang-xi Z. 2009. Study on the reaction degree of calcined coal gangue powder in blended cement by selective solution method. *J. Procedia Earth and Planetary Science*, 1(1):634-639. <https://doi.org/10.1016/j.proeps.2009.09.100>
 7. Addou R, Hannawi K, Agbodjan WP, Zenasni M. 2015. Caractérisation des déchets stériles de charbon de la mine de Jerada (Est du Maroc), en vue de l'élaboration d'un éco-matériau en génie civil. *Mécanique et Electrique pour l'Energie (CMEEE 2015)*.
 8. Xu H, Song W, Cao W, Shao G, Lu H, Yang D, Chen D, Zhang R. 2017. Utilization of coal gangue for the production of brick. *J. Material cycles and waste management*. 19:1270-1278. <https://doi.org/10.1007/s10163-016-0521-0>
 9. Yang M, Guo Z, Deng Y, Xing X, Qiu K, Long J, Li J. 2012. Preparation of CaO-Al₂O₃-SiO₂ glass ceramics from coal gangue. *Int. J. Miner. Process*, 102:112-115. <https://doi.org/10.1016/j.minpro.2011.11.004>
 10. Cembureau and the United Nations, Cementing the European Green Deal. Reaching climate neutrality along the cement and concrete value chain by 2050. Retrieved from https://cembureau.eu/media/kuxd32gi/cembureau-2050-roadmap_final-version_web.pdf
 11. Zhao H, Zhang N, Wang HJ. 2014. Power consumption prediction modeling of cement manufacturing based on the improved multiple non-linear regression algorithm. *Appl. Mech. Mater.* 687:5185-5189. <https://www.scientific.net/AMM.687-691.5185>
 12. Rahman A, Rasul MG, Khan MMK, Sharma S. 2015. Recent development on the uses of alternative fuels in cement manufacturing process. *J. Fuel*. 145:84-99. <https://doi.org/10.1016/j.fuel.2014.12.029>
 13. Kermeli K, Edelenbosch OY, Crijns-Graus W, van Ruijven BJ, Mima S, van Vuuren DP, Worrell E. 2019. The scope for better industry representation in long-term energy models: Modeling the cement industry. *J. Appl. Energy*. 240:964-985. <https://doi.org/10.1016/j.apenergy.2019.01.252>
 14. International Energy Agency. 2023. World energy outlook. Retrieved from <https://iea.blob.core.windows.net/assets/86ede39e-4436-42d7-ba2a-edf61467e070/WorldEnergyOutlook2023.pdf>
 15. Belkheiria D, Diouri A, Taibi M, Sassi O, Aride J. 2015. Recycling of Moroccan coal gangue in the elaboration of a Portland clinker. *J. Mater. Environ. Sci.* 6(6):1570-1577.
 16. Chhaiba S, Blanco-Varela MT, Diouri A. 2018. Moroccan oil shale and coal waste as alternative raw materials in Portland cement clinker manufacture. Clinkerisation reactions and clinker characterisation. *J. Materiales de Construcción*. 68(331):e166. <https://doi.org/10.3989/mc.2018.07017>
 17. Wang XT, Lu B, Xu L, Li CY, Lin L, Huang J. 2013. Lower heating value estimation of coal gangue through proximate analysis data based on GB/T 212-2008. *J. Advanced Materials Research*. 726:2699-2703. <https://doi.org/10.4028/www.scientific.net/AMR.726-731.2699>
 18. Taha Y, Elghali A, Derhy M, Amrani M, Hakkou R, Benzaazoua, M. 2023. Towards an integrated approach for zero coal mine waste storage: solutions based on materials circularity and sustainable resource governance. *Mineral Processing and Extractive Metallurgy Review*. 44(6):375-388. <https://doi.org/10.1080/08827508.2022.2084733>
 19. Taha Y, Benzaazoua M, Hakkou R, Mansori M. 2017. Coal mine wastes recycling for coal recovery and eco-friendly bricks production. *J. Miner. Eng.* 107:123-138.
 20. <https://doi.org/10.1016/j.mineng.2016.09.001>
 21. Kuntze, R.A. 2009. Gypsum: Connecting Science and Technology. ASTM MNL 67, ASTM International.
 22. Gunasekaran S, Anbalagan G. 2007. Thermal decomposition of natural dolomite. *J. B. Mater. Sci.* 30:339-344. <https://doi.org/10.1007/s12034-007-0056-z>
 23. Gualtieri AF, Ferrari S. 2006. Kinetics of illite dehydroxylation. *J. Phys.Chem.Miner.* 33:490-501. <https://doi.org/10.1007/s00269-006-0092-z>
 24. Kaantee U, Zevenhoven R, Backman R, Mikko H. 2003. Modelling a cement manufacturing process to study possible impacts of alternative fuels. *Ciments Betons Platres Chaux*. 46-52.
 25. Mohalik NK, Mandal S, Ray SK, Khan AM, Mishra D, Pandey JK. 2022. TGA/DSC study to characterise and classify coal seams conforming to susceptibility towards spontaneous combustion. *Int. J. Min. Sci. Technol.* 32(1):75-88. <https://doi.org/10.1016/j.ijmst.2021.12.002>
 26. McBride BJ. 2002. NASA Glenn coefficients for calculating thermodynamic properties of individual species. National Aeronautics and Space Administration, John H. Glenn Research Center at Lewis Field.
 27. Blanc P, Vieillard P, Gailhanou H, Gaboreau S, Gaucher E, Fialips CI, Made B, Giffaut E. 2015. A generalized model for predicting the thermodynamic properties of clay minerals. *Am. J. Sci.* 315(8):734-780. <https://doi.org/10.2475/08.2015.02>
 28. Gottschalk M. 1997. Internally Consistent Thermodynamic Data for rock-forming minerals in the system SiO₂-TiO₂-Al₂O₃-Fe₂O₃-CaO-MgO-FeO-K₂O-Na₂O-H₂O-CO₂. *Eur. J. Mineral.* 9:175-223 cp dolomite.
 29. Leśniak B, Lukasz S, Jakubina G. 2013. Institute for chemical processing of coal, zabrze, poland. The determination of the specific heat capacity of coal based on literature data. *Chemik.* 67(6):560-571.
 30. Eisermann W, Johnson P, Conge, WL. 1980. Estimating thermodynamic properties of coal, char, tar and ash. *Fuel Process. Technol.* 3(1):39-53. [https://doi.org/10.1016/0378-3820\(80\)90022-3](https://doi.org/10.1016/0378-3820(80)90022-3)
 31. Lothenbach B, Matschei T, Möschner G, Glasser FP. 2008. Thermodynamic modelling of the effect of temperature on the hydration and porosity of Portland cement. *Cem. Concr. Res.* 38(1):1-18. <https://doi.org/10.1016/j.cemconres.2007.08.017>
 32. Thoenen T, Kulik D. 2003. Nagra/PSI chemical thermodynamic database 01/01 for the GEM-Selektor (V. 2-PSI) geochemical modeling code. PSI, Villigen. https://doi.org/10.1524/ract.2002.90.9-11_2002.805
 33. Hummel W, Berner U, Curti E, Pearson FJ, Thoenen T. 2002. Chemical thermodynamic data base (01/01). Nagra/PSI Chemical Thermodynamic Data Base, 1(01):565. https://doi.org/10.1524/ract.2002.90.9-11_2002.805
 34. Hanein T, Glasser FP, Bannerman MN.2020. Thermodynamic data for cement clinkering. *J. Cement and Concrete Research*. 132:106043. <https://doi.org/10.1016/j.cemconres.2020.106043>
 35. Haas Jr JL, Robinson Jr GR, Hemingway BS. 1981. Thermodynamic tabulations for selected phases in the system CaO-Al₂O₃-SiO₂-H₂ at 101.325 kPa (1 atm) between 273.15 and 1800 K. *J. Phys. Chem. Ref. Data.* 10(3):575-670. <https://doi.org/10.1063/1.555645>
 36. Bonnicksen KR. 1955. High temperature heat contents of aluminates of calcium and magnesium. *J. Phys. Chem.* 59(3):220-221. <https://doi.org/10.1021/j150525a006>.
 37. Babushkin VI, Matveev GM, Mchedlov-Petrosian OP. 1985. Thermodynamics of silicates.
 38. Chellai H, Essamoud R, Rjimati E. 2011. Le bassin houiller de Jerada (Chaîne des Horsts, Maroc oriental) / The Jerada Coal Basin (Horst Chain, Eastern Morocco). 1(556-564):331-335.
 39. Darmane Y, Alaoui A, Kitane S, Bennajah M, Daramy A, Cherkaoui M. 2009. Recycling the slagheap of an old coal mine (Morocco). *Sep. Purif. Technol.* 68(1):125-128. <https://doi.org/10.1016/j.seppur.2009.04.026>

40. Shen J, Zhu S, Liu X, Zhang H, Tan, J. 2010. The prediction of elemental composition of biomass based on proximate analysis. *Energy Convers. Manag.* 51(5):983-987. <https://doi.org/10.1016/j.enconman.2009.11.039>
41. Lawal AI, Aladejare AE, Onifade M, Bada S, Idris MA. 2021. Predictions of elemental composition of coal and biomass from their proximate analyses using ANFIS, ANN and MLR. *Int. J. Coal Sci. Technol.* 8:124-140.
42. Shim SH, Lee TH, Yang SJ, Noor NBM, Kim JHJ. 2021. Calculation of cement composition using a new model compared to the bogue model. *Materials.* 14(16):4663. <https://doi.org/10.3390/ma14164663>
43. Belkheiri D, Taibi M, Diouri A, Boukhari A, Aride A, Sassi O. 2014. Characterization of Moroccan coal waste: valorization in the elaboration of the Portland clinker. *MATEC Web of Conferences* 11:01009. <https://doi.org/10.1051/mateconf/20141101009>.